JOURNAL OF MATERIALS SCIENCE 26 (1991) 4225–4233

Chemical and structural properties of the system Fe_2O_3–In_2O_3

M. RISTIĆ, S. POPOVIĆ*, M. TONKOVIĆ, S. MUSIĆ
*Rudjer Bošković Institute, P.O. Box 1016, and * Department of Physics, Faculty of Science, University of Zagreb, P.O. Box 162, 41001 Zagreb, Croatia, Yugoslavia*

The system Fe_2O_3–In_2O_3 was studied using X-ray diffraction, ^{57}Fe Mössbauer spectroscopy and infrared spectroscopy. The samples were prepared by chemical coprecipitation and thermal treatment of the hydroxide coprecipitates. For samples heated at 600 °C, a phase, α-$(Fe_{1-x}In_x)_2O_3$, isostructural with α-Fe_2O_3, exists for $0 \leqslant x \lesssim 0.8$, and a phase C-$(Fe_{1-x}In_x)_2O_3$, isostructural with cubic In_2O_3, exists for $0.3 \lesssim x \leqslant 1$. In the two-phase region these two phases are poorly crystallized. An amorphous phase is also observed for $0.3 \lesssim x \lesssim 0.7$. For samples heated at 900 °C the two-phase region is wider and exists for $0.1 \lesssim x \lesssim 0.8$ with the two phases well crystallized. In these samples an amorphous phase is not observed. ^{57}Fe Mössbauer spectroscopy of samples prepared at 600 °C indicated a general tendency of the broadening of spectral lines and the decrease of numerical values of the hyperfine magnetic field (HMF) with increasing molar fraction In_2O_3 in the system Fe_2O_3–In_2O_3. The samples prepared at 900 °C, in the two-phase region, are characterized by a constant HMF value of 510 kOe at room temperature. Infrared spectroscopy was also used to follow the changes in the infrared spectra of the system Fe_2O_3–In_2O_3 with gradual increase of molar fraction of In_2O_3. A correlation between X-ray diffraction, Mössbauer spectroscopic and infrared spectroscopic results was obtained.

1. Introduction

α-Fe_2O_3, haematite, is isostructural with α-Al_2O_3, corundum. Also, haematite is characterized by a specific magnetic behaviour [1]: it is paramagnetic above the Curie temperature ($T_C \sim 955$ K for pure bulk α-Fe_2O_3), weakly ferromagnetic between T_C and the Morin transition ($T_M \sim 260$ K for pure bulk α-Fe_2O_3) and antiferromagnetic below the Morin transition. Structural, magnetic and electric properties of haematite have been the subjects of numerous investigations.

Chadwick *et al.* [2] prepared iron oxides from $Fe(NO_3)_3 \cdot 9H_2O$ salt under a variety of conditions using a simple hydrolysis and thermal treatment of the samples. The analysis of samples showed the presence of α-Fe_2O_3 and ferrihydrite, which can be considered to be a disordered haematite with water molecules being an integral part in the structure. Mössbauer spectroscopy did not show the relaxation effects in haematite. On the other hand, the ferrihydrite component clearly exhibited the effects of magnetic relaxation.

In the haematite structure, the Fe^{3+} ions can be partially replaced with other metal cations, for instance with Al^{3+} ions. The percentage of substitution of Fe^{3+} ions with other metal cations varies depending on the nature of the substituting cation. Such a substitution can affect significantly the structural, magnetic and electric properties of haematite.

Fysh and Clark [3] calculated the recoil-free fraction at room temperature, for pure haematite and for haematite containing 14 mol% Al. The recoil-free fraction increased from 0.64 for pure α-Fe_2O_3 to 0.82 for α-$(Fe_{1-x}Al_x)_2O_3$, where x corresponds to 14 mol % Al.

Murad [4] investigated the influence of Al substitution on the absorption of 14.4 keV γ-rays in haematite. He also found that the absorption of γ-rays increased with substitution of Fe^{3+} by Al^{3+}.

Fysh and Fredericks [5] applied Fourier transform infrared spectroscopy (FTIR) in the study of aluminous haematites and goethites. For high-temperature aluminous haematites, a linear relationship exists between Al content and the location of the band near 470 cm^{-1}, up to 10 mol % Al substitution. The FTIR spectra of haematite produced by calcining the goethite at 590 °C showed a strong dependence of the band position and intensity on the goethite method of preparation.

Barron *et al.* [6] found that the characteristic shifts in the infrared spectra of aluminous haematites depended on the content of aluminium. However, these infrared shifts can be affected by the morphology of particles.

Murad and Schwertmann [7] studied the influence of the Al substitution and crystal size on the Mössbauer spectrum of haematite at room temperature. They observed that the hyperfine magnetic field decreased both with increasing Al-for-Fe substitution and with decreasing crystal size. The decrease of the hyperfine magnetic field values was accompanied by broadening of the Mössbauer lines. Mössbauer spectroscopy was also used [8] as a technique for the

0022–2461/91 $03.00 + .12 © *1991 Chapman and Hall Ltd.*

quantitative determination of the aluminium-substituted goethite–haematite mixtures.

The synthetic Mn-substituted goethites, α-$(Fe_{1-x}Mn_x)OOH$, and haematites, α-$(Fe_{1-x}Mn_x)_2O_3$, with x up to 0.08, were studied by ^{57}Fe Mössbauer spectroscopy [9]. The hyperfine magnetic field is found to be less influenced by Mn substitution, than in the case of Al. It was also found that Mn substitution suppressed drastically the Morin transition in haematite, which resulted in a weakly ferromagnetic state at 80 K for compositions with $x > 0.04$.

De Grave *et al.* [10] studied the effect of crystallinity and Al substitution on the magnetic properties and the Morin transition in haematite. The pore-containing particles disappeared gradually with increasing heating temperature, and this caused the Morin transition temperature to shift to higher values. De Grave *et al.* also suggested that the two low-temperature phases, observed in the Mössbauer spectra, coexisted within the particles and that the canting of the spins with respect to the crystallographic axes can be ascribed to the magnetic exchange interactions, which favour a uniform spin orientation within the same particles.

Recently, Musić *et al.* [11] published the results of an investigation of the system Fe_2O_3–Ga_2O_3 using X-ray diffraction and ^{57}Fe Mössbauer spectroscopy. The presence of only α-$(Fe_{1-x}Ga_x)_2O_3$ phase was detected for the compositions with x between 0 and ~ 0.90. A gradual decrease of the unit-cell parameters of α-$(Fe_{1-x}Ga_x)_2O_3$ and the reduction of the hyperfine magnetic field with the increasing gallium substitution were measured. The hyperfine magnetic structure, which was observed for α-$(Fe_{1-x}Ga_x)_2O_3$ at room temperature, collapsed for the composition with $x \sim 0.50$.

In the present publication we report the results of an investigation of the system Fe_2O_3–In_2O_3 using X-ray diffraction, ^{57}Fe Mössbauer spectroscopy and infrared spectroscopy as experimental techniques. $_{49}In$ belongs to the group of elements in the periodic system, in which there are also $_5B$, $_{13}Al$, $_{31}Ga$ and $_{81}Tl$. The ionic radius in the trivalent state of these elements increases with the atomic number, for instance 0.057 nm for Al^{3+}, 0.062 nm for Ga^{3+} and 0.092 nm for In^{3+}. Chemistry of Ga^{3+} and In^{3+} shows many similarities. However, In^{3+} (0.092 nm) has significantly greater ionic radius than Fe^{3+} (0.067 nm). For this reason, we expected different effects of the In^{3+} ions on the haematite structure in relation to the Ga^{3+} ions.

2. Experimental procedure

Analar reagent grade chemicals and doubly distilled water were used. The $Fe(OH)_3$–$In(OH)_3$ coprecipitates were carefully washed and then dried. Twelve samples, S-1 to S-12 were obtained by heating the corresponding hydroxide coprecipitates for 1 h at 200 °C, for 1 h at 300 °C, for 1 h at 400 °C and for 5 h at 600 °C ("step-by-step" heating). The chemical composition of samples S-1 to S-12 is given in Table I. Samples S-1 to S-12 were additionally heated for 6 h at 900 °C. The samples obtained at 900 °C are denoted by an asterisk, S-1* to S-12*.

TABLE I Chemical composition of the samples in the system Fe_2O_3–In_2O_3

Sample	Molar fractions	
	Fe_2O_3	In_2O_3
S-1	0.99	0.01
S-2	0.97	0.03
S-3	0.95	0.05
S-4	0.90	0.10
S-5	0.85	0.15
S-6	0.80	0.20
S-7	0.70	0.30
S-8	0.50	0.50
S-9	0.30	0.70
S-10	0.10	0.90
S-11	0.05	0.95
S-12		1.00

X-ray diffraction measurements were performed using a counter diffractometer with monochromatic Cu$K\alpha$ radiation (Philips diffractometer, proportional counter and graphite monochromator).

Mössbauer spectra were recorded using a commercial Mössbauer spectrometer by Wissel. A ^{57}Co–Rh source was used. The standard absorbers, α-Fe, α-Fe_2O_3 and ^{57}Fe–Rh were also used.

The infrared spectra were recorded using a 580 B Perkin–Elmer spectrometer. The specimens were pressed in KBr discs.

3. Results and discussion

3.1. X-ray diffraction

The crystallographic data for α-Fe_2O_3 and cubic C-In_2O_3 are shown in Table II. In the present work, the system Fe_2O_3–In_2O_3 was investigated by X-ray diffraction over the whole concentration range. The X-ray diffraction results can be summarized as follows.

For samples heated to 600 °C a phase α-$(Fe_{1-x}In_x)_2O_3$, α_S, isostructural with α-Fe_2O_3, exists for $0 \leqslant x \lesssim 0.8$ (samples S-1 to S-9), and a phase C-$(Fe_{1-x}In_x)_2O_3$, C_S, isostructural with cubic In_2O_3, exists for $0.3 \lesssim x \leqslant 1$ (samples S-7 to S-12). In the two-phase region these two phases are poorly crystallized. For $0.3 \lesssim x \lesssim 0.7$ (samples S-7 to S-9) an amorphous fraction is also present.

In the single-phase regions a shift of diffraction lines toward smaller θ values takes place, due to a gradual replacement of Fe with In. The corresponding increase of the lattice parameters of the α_S-phase from $x = 0$ to $x \sim 0.3$ amounts to 1.1%, and the increase of the lattice parameter of the C_S phase from $x \sim 0.8$ to $x = 1$ is 1.0%. Sample S-7 is very poorly crystallized, while samples S-8 and S-9 exhibit very broad diffraction lines. Broadening of diffraction lines is also observed for samples S-5 and S-6 and S-10 to S-12. A characteristic part of the X-ray powder diffraction pattern of sample S-8 is shown in Fig. 1.

For the samples additionally heated at 900 °C the results are similar to those obtained for the samples heated up to 600 °C. The two-phase region is wider

TABLE II Crystal data for α-Fe_2O_3 and cubic C-In_2O_3

JCPDS PDF card no. [24]	Compound	Space group	Unit-cell parameters (nm)
			hexagonal axes
13-534	α-Fe_2O_3	$R\bar{3}c$ (167)	$a = 0.5034$
			$c = 1.3752$
6-416	C-In_2O_3	$I2_13$(199)	$a = 1.0118$

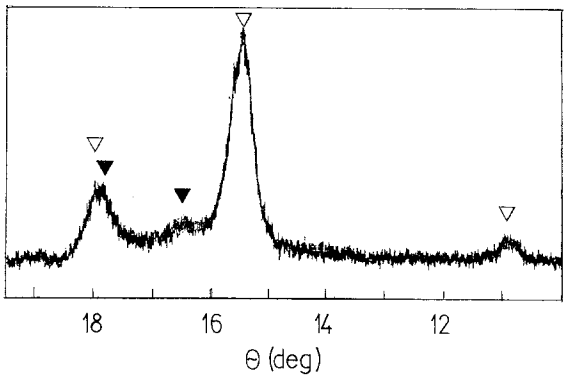

Figure 1 Characteristic part of X-ray powder diffraction pattern of sample S-8 (50 mol% Fe_2O_3 + 50 mol% In_2O_3). Radiation: monochromatic CuK_α. Phases: (▼) α_S, isostructural with α-Fe_2O_3, (▽) C_S, isostructural with cubic C–In_2O_3.

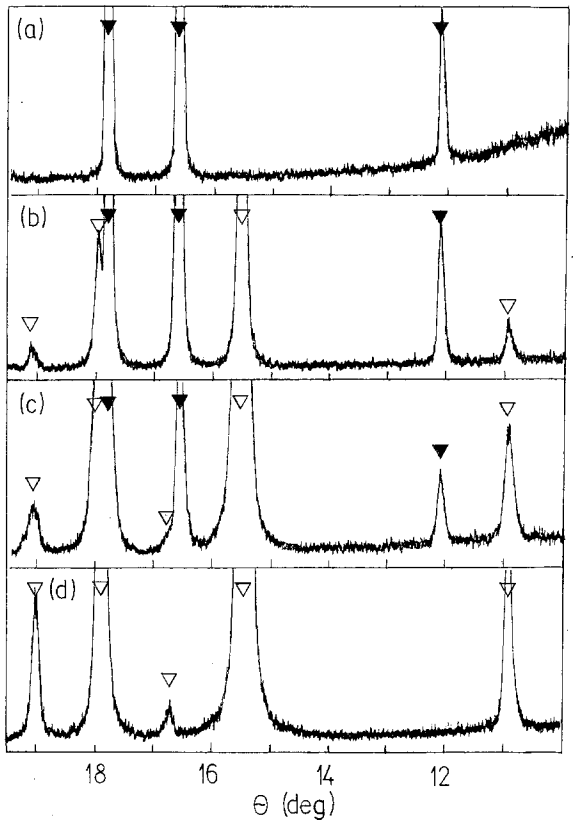

Figure 2 Characteristic parts of X-ray diffraction patterns of samples (a) S-1*, (b) S-6*, (c) S-8* and (d) S-11*. These samples were obtained at 900 °C. Radiation: monochromatic CuK_α. Phases: (▼) α_S, isostructural with α-Fe_2O_3 (▽) C_S, isostructural with cubic C-In_2O_3.

and exists for $0.1 \lesssim x \lesssim 0.8$ (samples S-4* to S-9*). The two phases, α_S and C_S, are well crystallized. Samples S-4* to S-9* exhibit only a small broadening of diffraction lines. No amorphous phase is present. The increase in the lattice parameters of the α_S-phase with x from $x = 0 - \sim 0.1$ amounts to 0.7%, and the increase of the lattice parameter of the C_S-phase from $x \sim 0.8$ to $x = 1$ amounts to 1.0%. In the two-phase region the diffraction lines of both α_S and C_S phases do not move with x in both cases, for samples heated to 600 °C and for those additionally heated at 900 °C. Characteristic parts of the X-ray powder diffraction patterns of samples S-1*, S-6*, S-8* and S-11* are shown in Fig. 2.

On the basis of the X-ray diffraction results it can be concluded that in the system Fe_2O_3–In_2O_3 solid solutions exist in narrow concentration regions, at the Fe-rich side and at the In-rich side. On the other hand, in the system Fe_2O_3–Ga_2O_3 [11] solid solutions appear over the whole concentration range, i.e. the phase α-$(Fe_{1-x}Ga_x)_2O_3$, isostructural with α-Fe_2O_3 and α-Ga_2O_3, exists from $x = 0 - \sim 0.95$, and β-$(Fe_{1-x}Ga_x)_2O_3$, isostructural with β-Ga_2O_3, for $x \gtrsim 0.95$. These effects can be attributed to a big difference between the ionic radii of Fe^{3+} and In^{3+} in the first case, and the similarity of the ionic radii of Fe^{3+} and Ga^{3+} in the second case.

3.2. ^{57}Fe Mössbauer spectroscopy

Fig. 3 shows the Mössbauer spectra of samples S-1, S-2, S-6 and S-7. In this figure the standard lines of well-crystallized α-Fe_2O_3 are also shown. The Mössbauer spectroscopic results indicate the general tendency of the broadening of Mössbauer lines and the decrease of the numerical values of the hyperfine magnetic field (HMF) with increasing of content of In^{3+} ions. Table III shows the average values of the hyperfine magnetic field calculated on the basis of recorded Mössbauer spectra for samples S-1 to S-6. Broadening of Mössbauer lines is very pronounced in the spectrum of sample S-6. Also, there is a gradual increase of the intensity of inner lines, particularly of lines 2 and 5. The Mössbauer spectrum of sample S-7 recorded at room temperature does not show hyperfine magnetic splitting; only the asymmetrical central doublet is observed. As already mentioned, for samples S-1 to S-6 only one phase, α-$(Fe_{1-x}In_x)_2O_3$, isostructural with α-Fe_2O_3, is observed by X-ray diffraction. For the same samples the Mössbauer spectra show hyperfine magnetic splitting at room temperature.

In the region of the formation of solid solution (samples S-1 to S-6) the In^{3+} ions are dissolved in the haematite structure. In these samples there is a non-uniform (statistical) distribution of In^{3+} ions. The presence of In^{3+} ions in a haematite structure affects the electronic environment of the ^{57}Fe resonant atoms, and this reflects on their contributions to the Mössbauer effect. Generally, the ^{57}Fe Mössbauer effect in the system Fe_2O_3–Me_2O_3 (Me^{3+} = metal cation) can be interpreted in the sense of the electronic relaxation and the superparamagnetism. Morup *et al.* [12] discussed the influence of substituting cations on the ^{57}Fe Mössbauer spectra of different iron oxides.

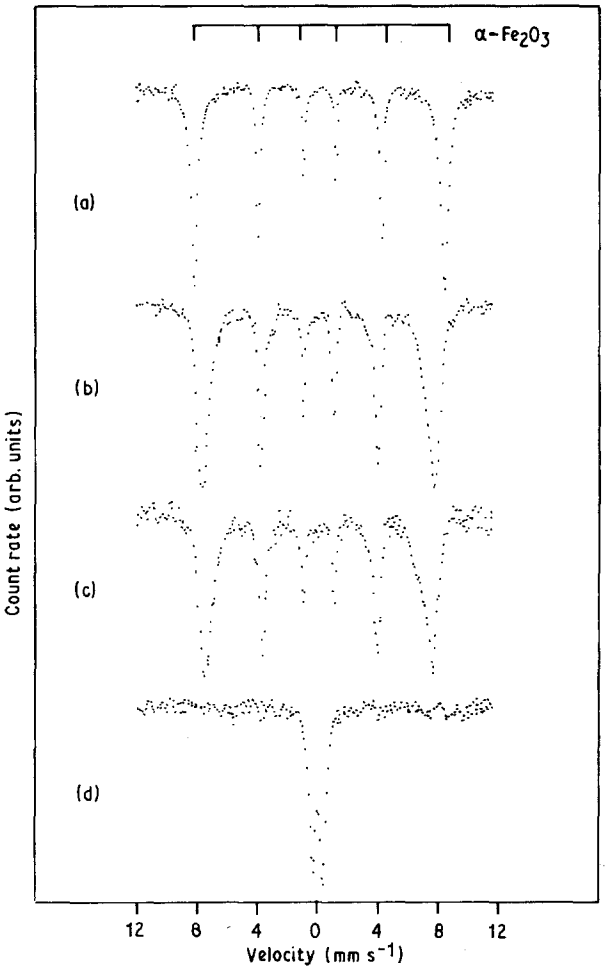

Figure 3 ^{57}Fe Mössbauer spectra of samples (a) S-1, (b) S-2, (c) S-6 and (d) S-7, recorded at room temperature.

TABLE III Hyperfine magnetic fields (average values) for samples S-1 to S-6 measured at room temperature

Sample	$H_{5/2}$ (kOe)
S-1	514
S-2	511
S-3	506
S-4	500
S-5	477
S-6	488

Fig. 4 shows the Mössbauer spectrum of sample S-8 recorded at room temperature. The asymmetry of the Mössbauer lines is pronounced and this spectrum can be regarded as a superposition of two doublets, Q_1 and Q_2. Their Mössbauer parameters are: $\delta_1 = 0.354\ \text{mm s}^{-1}$, $\Delta_1 = 0.758\ \text{mm s}^{-1}$, $\delta_2 = 0.337\ \text{mm s}^{-1}$ and $\Delta_2 = 0.999\ \text{mm s}^{-1}$. Isomer shifts, δ_1 and δ_2, are given relative to α-Fe. This result indicates the presence of the ^{57}Fe resonant atoms in different structural environments, which is in agreement with the X-ray diffraction results. Fig. 5 shows the ^{57}Fe Mössbauer spectra of samples S-9, S-10 and S-11 recorded at room temperature. These spectra are characterized with the asymmetrical doublet, and they are similar to the spectrum of sample S-8.

The additional heating of the samples at 900 °C produced significant changes in the corresponding

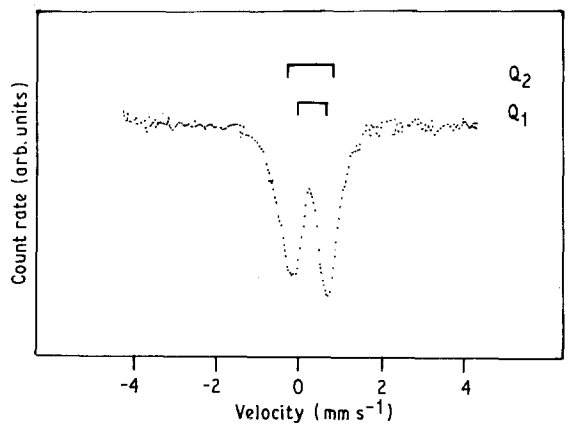

Figure 4 ^{57}Fe Mössbauer spectrum of sample S-8, recorded at room temperature.

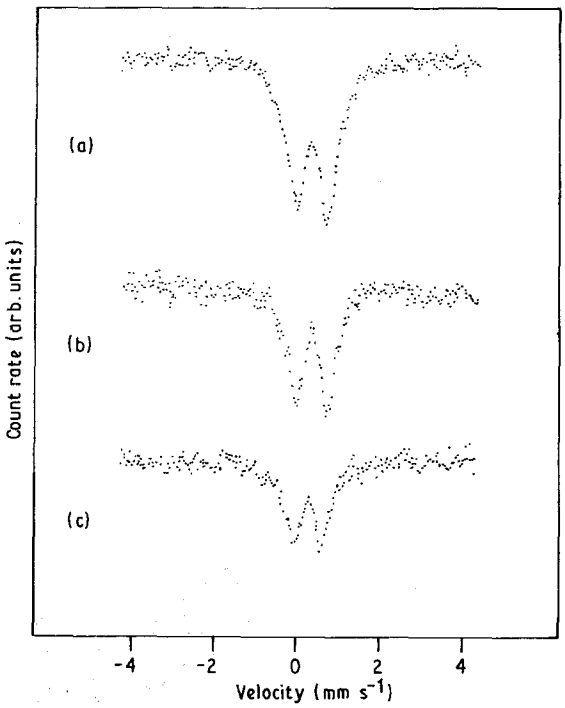

Figure 5 ^{57}Fe Mössbaur spectra of samples (a) S-9, (b) S-10 and (c) S-11, recorded at room temperature.

TABLE IV Hyperfine magnetic fields (average values) for samples S-1* to S-9* measured at room temperature

Sample	$H_{5/2}$ (kOe)
S-1*	517
S-2*	517
S-3*	510
S-4*	510
S-5*	510
S-6*	510
S-7*	510
S-8*	510
S-9*	508
S-10*	No hyperfine magnetic splitting

Mössbauer spectra. Fig. 6 shows the ^{57}Fe Mössbauer spectra of samples S-1* to S-10* recorded at room temperature. Hyperfine magnetic fields (average values), for samples S-1* to S-9*, are given in Table IV.

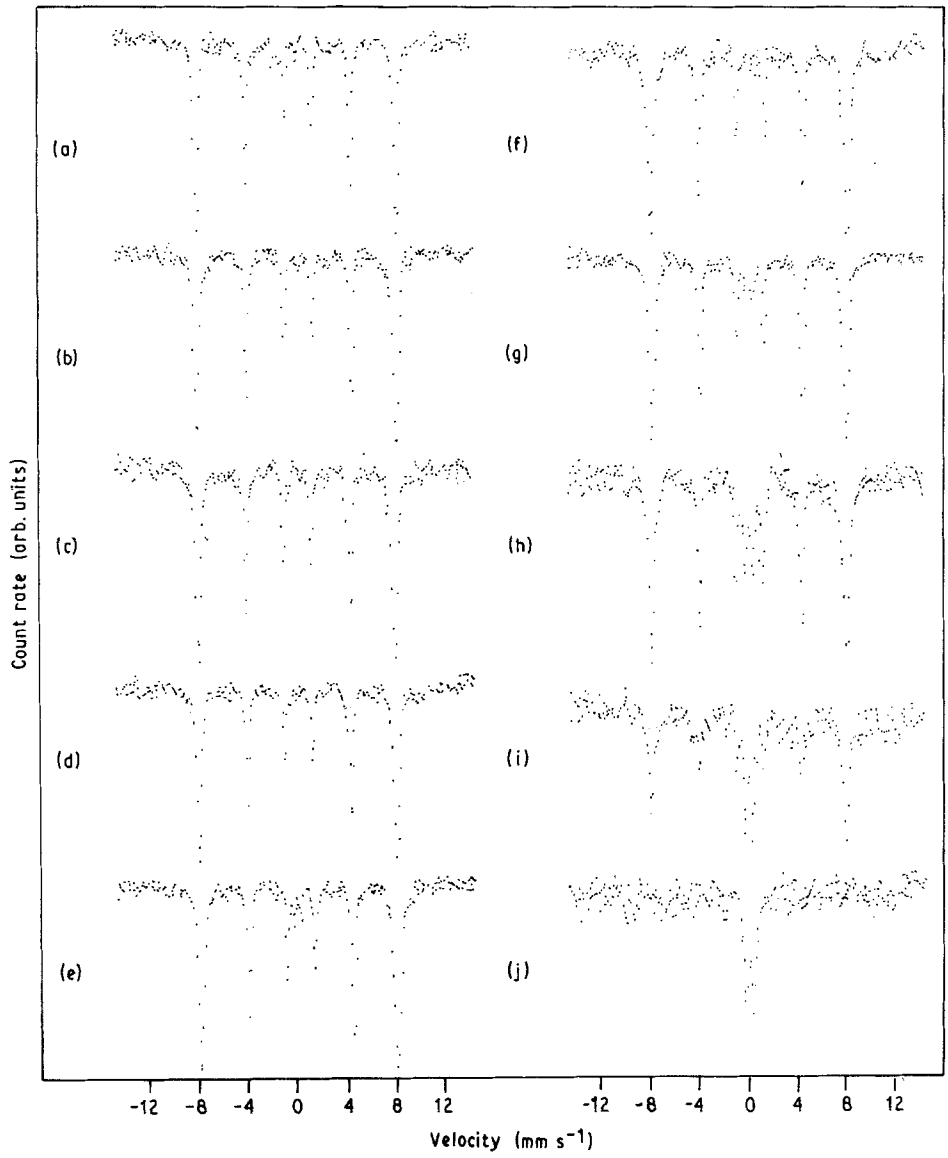

Figure 6 ^{57}Fe Mössbauer spectra of samples S-1* to S-10*, recorded at room temperature. (a) S-1*, (b) S-2*, (c) S-3*, (d) S-4*, (e) S-5*, ((f) S-6*, (g) S-7*, (h) S-8*, (i) S-9*, (j) S-10*..

The hyperfine magnetic splitting spectra, without a central quadrupole doublet, are recorded for samples S-1* to S-6*. A central quadrupole doublet of very small intensity is observed in the Mössbauer spectrum of sample S-7*, whereas the relative intensity of the central quadrupole doublet is bigger in samples S-8* and S-9*. The Mössbauer spectrum of sample S-10* shows only the asymmetrical quadrupole doublet. The hyperfine magnetic field of samples S-1* and S-2* is 517 kOe. This value of HMF is generally

TABLE V Characteristic infrared absorption bands observed for different haematite samples (literature data)

Sample	Infrared absorption bands (cm^{-1})										Reference
Haematite				560	468		370	325			[13]
				540	470			345			[14]
"Protohaematite"				530		445			305, 297		
				530		445	390		308	233	[15]
Haematite				543	468			333		233–240	
"Protohaematite"			640	525			395		295		[16]
Haematite				542	470		380	340			
"Hydrohaematite"	3400	950	630	540	470		385	330	300	230	[17]
Haematite				540	470	440	385	325		230	
Haematite	(TO)[a]	299	526	227	286	437	524				[18]
	(LO)[b]	414	662	230	368	494	662				
Haematite –	observed	–	575	485	385	360	–				
sphere	estimated	585	595	485	386	358	230				
Haematite –	observed	650	525	440	–	300	–				
lath	estimated	660	525	440	412	296	230				[19]

[a] Transverse-optical-phonon frequencies.
[b] Longitudinal-optical-phonon frequencies.

measured for the well-crystallized haematite. Samples S-3* to S-8* are characterized by a constant HMF value of 510 kOe and for sample S-9* this value is little reduced (508 kOe). These results can be connected to the X-ray diffraction results, which showed, for samples S-4* to S-9*, the presence of the two-phase region and that in this region the diffraction lines of both α_S and C_S phases do not move with x.

3.3. Infrared spectroscopy

The infrared spectrum of haematite has been extensively investigated by many researchers. Table V shows the characteristic infrared absorption bands (cm^{-1}) observed for haematite samples.

McDevitt and Baun [13] published the characteristic infrared bands of haematite at 560, 480, 370 and 325 cm^{-1}. Schwertmann and Taylor [14] suggested that characteristic infrared bands at 540, 470 and 345 cm^{-1} in the low-frequency region can be used as fingerprints in the identification of a haematite. Differences in the location of the characteristic infrared bands of natural haematite can be ascribed to the presence of foreign ions in the haematite structure. Also, the degree of crystallinity strongly affects the infrared spectrum of haematite.

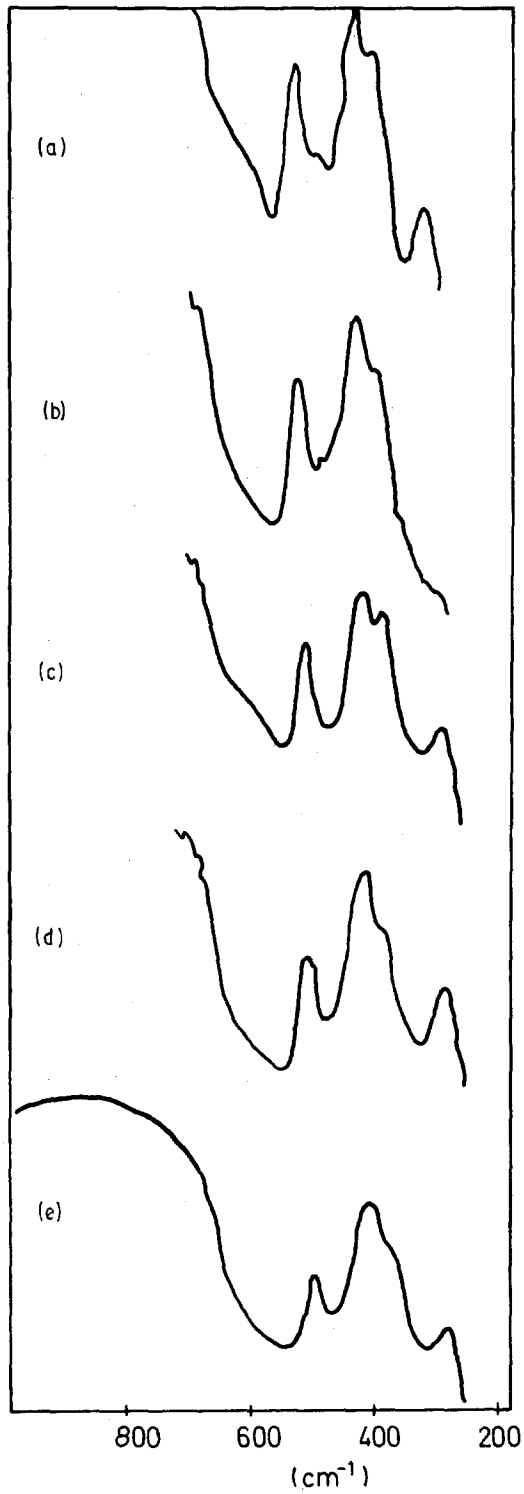

Figure 7 Characteristic parts of the infrared spectra recorded for samples (a) α-Fe_2O_3, (b) S-1, (c) S-3, (d) S-4 and (e) S-5.

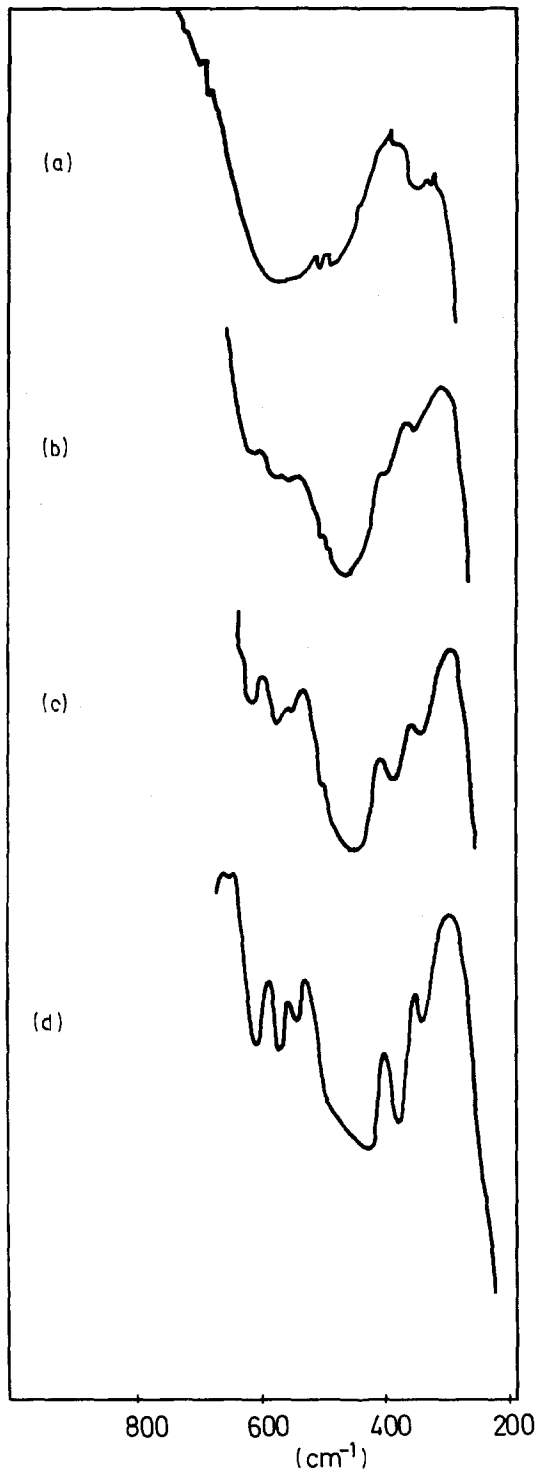

Figure 8 Characteristic parts of the infrared spectra recorded for samples (a) S-7, (b) S-8, (c) S-9 and (d) S-12.

TABLE VI Characteristic infrared bands (cm^{-1}) measured for samples α-Fe_2O_3 and S-1 to S-12

α-Fe_2O_3	S-1	S-2	S-3	S-4	S-5	S-6	S-7	S-8	S-9	S-10	S-11	S-12
								605 vw	605 w	605 m	605 m	605 m
535 s	540 s	538 s	530 s	535 s	530 s	535 s	560 s, b	570 sh	565 w	570 m	565 m	565 m
								540 sh	540 sh	540 sh	540 w	538 w
470 sh	470 m	465 m	460 s	465 m	460 m	460 m	470 m,b	450 s	440 s	430 s	420 vs	420 vs
445 m												
380 sh	380 sh	380 vw	380 vw	380 sh				380 sh	375 m	375 m	370 m	370 m
320 m	310 sh	310 w	305 m	315 m	310 m	305 w	330 w,b	335 vw	335 w	340 sh	330 w	330 m

s = strong, m = medium, w = weak, vw = very weak, sh = shoulder, b = broad.

Yariv and Mendelovici [15] investigated the effect of the degree of crystallinity on the infrared spectrum of haematite. In their paper, the poorly crystalline haematite was termed "protohaematite", whereas well crystalled oxide produced at temperatures above 700 °C was haematite. The infrared spectrum of "protohaematite" is characterized by three strong absorption bands at 530, 445 and 308 cm^{-1}, which were assigned to O^{2-} displacements. When the infrared discs were prepared without grinding, the infrared spectrum of "protohaematite" showed a doublet at 305 and 297 cm^{-1}. Infrared absorption bands at 543,

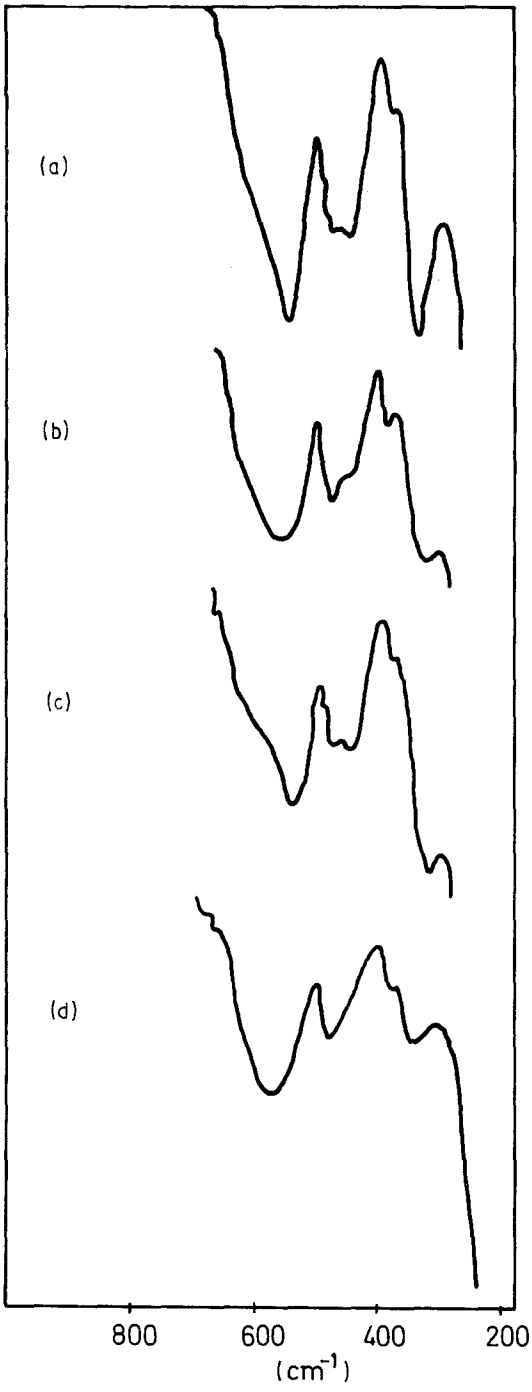

Figure 9 Characteristic parts of the infrared spectra recorded for samples (a) α-$Fe_2O_3^*$, (b) S-1*, (c) S-3* and (d) S-4*.

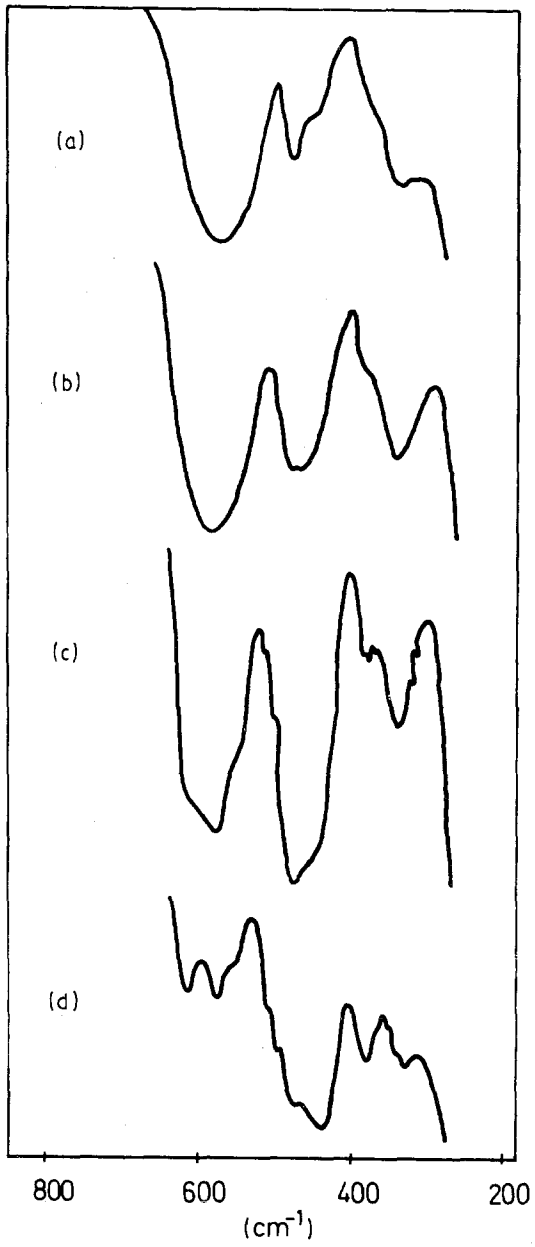

Figure 10 Characteristic parts of the infrared spectra recorded for samples (a) S-5*, (b) S-7*, (c) S-8* and (d) S-9*.

TABLE VII Characteristic infrared bands (cm^{-1}) measured for samples α-$Fe_2O_3^*$ and S-1* to S-11*

α-$Fe_2O_3^*$	S-1*	S-2*	S-3*	S-4*	S-5*	S-6*	S-7*	S-8*	S-9*	S-10*	S-11*
								605 sh	605 m	610 s	605 s
540 s	560 s	570 s		570 s	570 s	575 s	585 s	580 s	570 m	570 m	570 s
			535 s			540 sh			540 sh	545 w	540 m
475 sh	475 m	480 m	475 sh	475 m	475 m	475 m	470 s	460 s	470 sh		470 sh
445 m	435 sh	440 sh	435 m		440 sh				430 s	425 s	425 vs
380 sh	380 vw	380 vw	375 sh	380 sh		380 sh	380 sh	380 vw	375 m	375 m	370 s
340 s	325 w	335 w	320 w	340 m	335 w	345 m	340 m	335 m	330 w	330 w	330 m

s = strong, m = medium, w = weak, vw = very weak, sh = shoulder.

468 and 333 cm^{-1} were recorded, when goethite or "protohaematite" was heated above 700 °C. The infrared band at 233–240 cm^{-1} was ascribed to Fe^{3+} displacement.

Mendelovici *et al.* [16] also investigated the solid state conversion of pure α-FeOOH into distinctive α-Fe_2O_3 using the dry grinding method. The effect of particle size on the infrared bands assigned to O^{2-} displacements was suggested.

Wolska and Szajda [17] suggested that the presence of hydroxyl groups in the haematite lattice ("hydrohaematite") is the major factor affecting the infrared spectrum of haematite. In a recent publication [20], Wolska also suggested that the differences between the infrared spectra and X-ray diffraction patterns have a structural, rather than morphological origin and that they are caused by the occurrence of water in the haematite crystal lattice.

On the other hand, Serna and co-workers emphasized the influence of the particle shape on the infrared spectrum of haematite [19, 21, 22]. Hayashi and Kanamori [23] found that the infrared transmission spectra of α-Fe_2O_3 microcrystals can be explained taking into account the optical anisotropy, particle size and broadening mechanisms.

In the present study we investigated the influence of In^{3+} to Fe^{3+} replacement on the changes in the infrared spectrum of haematite. The characteristic parts of the infrared spectra, recorded for α-Fe_2O_3 and samples S-1, S-3 to S-5, S-7 to S-9 and S-12, are shown in Figs 7 and 8. The numerical values of the corresponding infrared bands (cm^{-1}) are given in Table VI. The results of these measurements can be summarized as follows. The strong absorption band at 530–540 cm^{-1} is broadened with increasing In^{3+} content. Replacement of Fe^{3+} with In^{3+} causes a shift of the infrared band at 455 cm^{-1} with a shoulder at 475 cm^{-1} to a position at 460–470 cm^{-1}. The infrared band at 320 cm^{-1} and a shoulder at 380 cm^{-1} are present in the spectra of all samples S-1 to S-6. However, the infrared band at 320 cm^{-1} becomes broader and shows a tendency to shift to the lower wave numbers as the In^{3+} content increases.

Significant changes in the infrared spectrum of sample S-7 were observed. This infrared spectrum is characterized by infrared bands which are very broad and poorly separated. The infrared bands at 535 and 320 cm^{-1} are shifted to 560 and 330 cm^{-1}, respectively. Evidently, infrared spectroscopy is sensitive to the structural changes in the system Fe_2O_3–In_2O_3. In a previous discussion, it was shown that in sample S-7, in addition to a phase α-$(Fe_{1-x}In_x)_2O_3$, there is also present a phase C-$(Fe_{1-x}In_x)_2O_3$ and an amorphous fraction. On the other hand, ^{57}Fe Mössbauer spectroscopy showed for sample S-7 the disappearance of the hyperfine magnetic field at room temperature.

In the infrared spectrum of sample S-8 (50 mol% Fe_2O_3 and 50 mol% In_2O_3), all the infrared bands characteristic of C-In_2O_3 (prepared at 600 °C) begin to appear (the infrared bands at 605, 570, 540, 380 and 330 cm^{-1}). The strong infrared band at 450 cm^{-1} is significantly broadened, while that at ~530–540 cm^{-1} disappears. In the infrared spectra of samples S-9 to S-12 the new infrared bands are more and more pronounced. The infrared band at 450 cm^{-1} (sample S-7) gradually shifts to 420 cm^{-1} (sample S-12) with increasing indium content.

Figs 9 and 10 show the characteristic parts of the infrared spectra of α-$Fe_2O_3^*$ and samples S-1*, S-3* to S-5* and S-7* to S-9*. The numerical values of the characteristic infrared bands (cm^{-1}) are given in Table VII.

Additional heating of α-Fe_2O_3 at 900 °C caused only a shift in the infrared band at 320 cm^{-1} to 340 cm^{-1}. The replacement of Fe^{3+} with In^{3+} caused a shift of the infrared band at 540 cm^{-1} to higher wave numbers. A weak or medium intensity band at ~310 cm^{-1} also shifts to higher wave numbers (325–345 cm^{-1}).

The thermal treatment of samples S-7 and S-8 at 900 °C caused changes in the corresponding infrared spectra. Generally, the spectral lines of these samples are more sharpened than those recorded for samples prepared at 600 °C. Also, the resolution of the infrared peaks increases from sample S-9* to S-11*. These effects can be ascribed to better crystallinity and the absence of amorphous phase.

References

1. E. MURAD and J. H. JOHNSON, in "Mössbauer Spectroscopy Applied to Inorganic Chemistry", Vol. II, edited by G. J. Long, (Plenum 1987) p. 507.
2. J. CHADWICK, D. H. JONES, M. F. THOMAS, G. J. TATLOCK and R. W. DEVENISH, *J. Magn. Magn. Mater.* **59** (1986) 301.
3. S. A. FYSH and P. E. CLARK, *Phys. Chem. Miner.* **8** (1982) 257.
4. E. MURAD, *Phys. Lett.* **111A** (1985) 79.
5. S. A. FYSH and P. M. FREDERICKS, *Clays Clay Miner.* **31** (1983) 377.
6. V. BARRON, J. L. RENDON, J. TORRENT and C. J. SERNA, *ibid.* **32** (1984) 475.
7. E. MURAD and U. SCHWERTMANN, *ibid.* **34** (1986) 1.

8. D. D. AMARASIRIWARDENA, E. de GRAVE, L. H. BOWEN and S. B. WEED, *ibid.* **34** (1986) 250.
9. R. E. VANDENBERGHE, A. E. VERBEECK, E. de GRAVE and W. STIERS, *Hyperfine Interact.* **29** (1986) 1157.
10. E. de GRAVE, L. H. BOWEN, R. VOCHTEN and R. E. VANDENBERGHE, *J. Magn. Magn. Mater.* **72** (1988) 141.
11. S. MUSIĆ, S. POPOVIĆ and M. RISTIĆ, *J. Mater. Sci.* **24** (1989) 2722.
12. S. MORUP, J. A. DUMESIC and H. TOPSOE, in "Application of Mössbauer Spectroscopy", Vol. II (Academic Press, New York, 1980) p. 1.
13. N. T. McDEVITT and W. L. BAUN, *Spectrochim. Acta* **20** (1964) 799.
14. U. SCHWERTMANN and R. M. TAYLOR, in "Minerals in Soil Environments" (Soil Science Society of America, Inc., Madison, WI, 1977) p. 145.
15. SH. YARIV and E. MENDELOVICI, *Appl. Spectrosc.* **33** 1979) 410.
16. E. MENDELOVICI, R. VILLALBA and A. SAGARZAZU, *Mater. Res. Bull.* **17** (1982) 241.
17. E. WOLSKA and W. SZAJDA, *J. Mater. Sci.* **20** (1985) 4407.
18. S. ONARI, T. ARAI and K. KUDO, *Phys. Rev. B* **16** (1977) 1717.
19. J. E. IGLESIAS and C. J. SERNA, *Miner. Petrogr. Acta* **29A** (1985) 363.
20. E. WOLSKA, *Sol. State Ionics* **28–30** (1988) 1349.
21. C. J. SERNA, J. L. RENDON and J. E. IGLESIAS, *Spectrochim. Acta* **38A** (1982) 797.
22. C. J. SERNA and J. E. IGLESIAS, *J. Mater. Sci. Lett.* **5** (1986) 901.
23. S. HAYASHI and H. KANAMORI, *J. Phys. C Solid State Phys.* **13** (1980) 1529.
24. International Centre for Diffraction Data, Joint Committee on Powder Diffraction Standards, Powder Diffraction File, Swarthmore, PA 19081, USA.

Received 21 December 1989
and accepted 2 August 1990